Progress In Electromagnetics Research M, Vol. 111, 65–76, 2022

Decoupling Control on Outer Rotor Coreless Bearingless Permanent Magnet Synchronous Motor Using LS-SVM Generalized Inverse

Zichen Zhang* **and Huangqiu Zhu**

Abstract—In order to solve the nonlinear couplings among speed and the radial displacement of the outer rotor coreless bearingless permanent magnet synchronous motor (ORC-BPMSM), a decoupling control strategy based on the least square support vector machine (LS-SVM) generalized inverse is proposed. Firstly, the basic structure and working principle of the ORC-BPMSM are introduced, and the mathematical model of torque and suspension forces are established. Secondly, the ORC-BPMSM system is proved reversible by establishing mathematical models and reversibility analysis, then the pseudo-linear subsystems are formed by connecting the generalized inverse system, which is identified by the LS-SVM, with the original system. Furthermore, additional closed-loop controllers are designed to improve the stability and robustness of the pseudolinear subsystems. Finally, the proposed method based on LS-SVM generalized inverse is compared with traditional inverse system method by simulations and experiments. The simulation and experiment results show that the proposed control strategy has good performance of decoupling and stability.

1. INTRODUCTION

Bearingless permanent magnet synchronous motor is a kind of high-performance motor integrating the characteristics of permanent magnet synchronous motors and magnetic bearings, which has the advantages of no friction, no lubrication and sealing, high speed, and high precision. It has potential application prospects in special electric transmission fields such as high-speed precision electric spindles, chemical pumps, and life sciences [1, 2]. With the development and utilization of new and renewable energy, the research and development of its energy storage system have become more and more important. Flywheel energy storage has received wide attention because of its advantages of high energy storage density, high energy conversion efficiency, low environmental impact, and long service life. The motor in a flywheel system, as a carrier of energy conversion, determines the performance of the flywheel energy storage system. Outer rotor coreless bearingless permanent magnet synchronous motor (ORC-BPMSM) has the advantages of no contact, no wear, no maintenance, and long service life which can meet the high-performance requirements of a flywheel energy storage system [3, 4].

ORC-BPMSM is a complex multivariable, nonlinear, and strong coupling system, and decoupling control is the premise of stable operation of the ORC-BPMSM. The generalized inverse system method can not only realize decoupling of the nonlinear system [5, 6], but also can make the decoupled subsystems open-loop stable. The poles of the subsystem are reasonably configured in the complex plane to obtain the ideal open-loop frequency characteristics.

It is important to establish an accurate mathematical model of the nonlinear system. In [7–11], neural networks are proposed to build the inverse system of the controlled model, but it is easy to fall into the problems of local optimum and slow convergence. Literature [12–15] use support vector machines to construct the inverse system of the controlled object. Support vector machines have good

Received 26 March 2022, Accepted 27 May 2022, Scheduled 19 June 2022
* Corresponding author: Zichen Zhang (18652738786@163.com).
The authors are with the School of Electrical and Information Engineering, Jiangsu University, Zhenjiang 212013, China.

nonlinear modeling and generalization capabilities, but it is limited by the computational complexity brought by solving quadratic programming problems. Least square support vector machine (LS-SVM) is firstly proposed by Vapnik [16] and Suykens [17], and the constraints in LS-SVM are all equation constraints, which can transform a nonlinear problem into a linear problem and make the fitted object close to the target object by the principle of minimizing the sum of squares of errors. Therefore, LS-SVM is faster, simpler, more accurate, and more widely used. Therefore, LS-SVM is combined with inverse system theory to realize decoupling control of nonlinear systems, and it is used to approximate the generalized inverse system of the ORC-BPMSM system and decouple the controlled object into the pseudo-linear subsystems.

In this paper, the LS-SVM generalized inverse model of the ORC-BPMSM with multivariate, nonlinear, and strong coupling is constructed, then it is connected in series with the original nonlinear multiple input output system to form a pseudo-linear system, and closed-loop controllers are designed. Finally, the effectiveness and reliability of the method are verified by simulation and experiment.

2. MATHEMATICAL MODEL AND GENERALIZED INVERSE OF THE ORC-BPMSM

2.1. Principle of Suspension Force Generation

The principle of the ORC-BPMSM suspension force generation is shown in Figure 1. In Figure 1(a), N_{Ma} and N_{Ba} are A-phase of torque windings and suspension force windings. The pole-pair number of torque windings is three, and the pole-pair number of suspension force windings is two. The solid line represents the 6-pole magnetic flux ψ_M generated by the permanent magnets and torque windings; the dotted line represents the 4-pole magnetic flux ψ_B generated by suspension force windings. Before the suspension force windings are supplied with current, the air gap magnetic flux is mainly composed of the magnetic flux generated by permanent magnets and torque windings. At this time, the magnetic field is balanced, and no suspension force is generated. When current is applied to suspension force windings, the generated magnetic flux produced by suspension force windings breaks the balance of the original air gap magnetic field. Because the directions of two kinds of fields in air gap 1 are the same, the field density increases. The situation is opposite in air gap 2, and the field density in air gap 2 decreases, thus a suspension force F_x is generated which is pointed to the positive x direction.

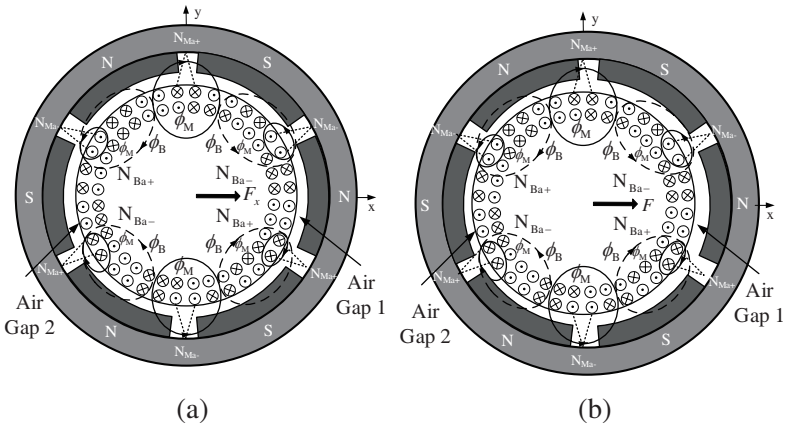

Figure 1. Generation principle of suspension force. (a) Suspension force. (b) Unbalance magnetic pull force.

In Figure 1(b), when the rotor is eccentrically displaced to right direction by the disturbing force, the balance of the air gap magnetic field will be broken, and the distribution of the air gap magnetic field will no longer be uniform. At this time, the magnetic flux density of the left side of the air gap magnetic field is greater than the right side, the rotor will move to right direction and collide with the bearing. In order to eliminate the effect of unbalanced magnetic pull force, the rotor can be brought back to the

equilibrium position by controlling the magnitude and direction of the current in the suspension force windings to change the air gap flux distribution and generate a left direction suspension force.

2.2. Mathematical Model

The magnitude of the suspension force is mainly determined by the eccentric displacement and interaction between the winding current and the magnetic field of the rotor. The calculation equations are

$$\begin{cases} F_x = K(i_{Bd}\psi_{Md} + i_{Bq}\psi_{Mq}) + Cx \\ F_y = K(i_{Bq}\psi_{Md} - i_{Bd}\psi_{Mq}) + Cy \\ T_e = 3P_M(\psi_{Md}i_{Mq} - \psi_{Mq}i_{Md})/2 \\ \psi_{Md} = L_{Md}i_{Md} + \psi_f \\ \psi_{Mq} = L_{Mq}i_{Mq} \end{cases} \tag{1}$$

where F_x and F_y are suspension forces in the x- and y-directions; x and y are the radial displacement of the rotor in the x- and y-directions; i_{Bd} and i_{Bq} are the current components of the suspension force windings in the d-q coordinate system; ψ_{Md} and ψ_{Mq} are the magnetic flux components of the torque windings and the permanent magnets in the d-q coordinate system, respectively; ψ_f is the magnetic of the permanent magnet; L_{Md} and L_{Mq}, i_{Md}, and i_{Mq} are the self-sensing and current components of the torque windings under the d-q coordinate system, respectively; P_M is the pole-pair number of torque windings; T_e is the electromagnetic torque; K and C are constant factors associated with the motor structure.

According to the Newtonian equation of motion, the rotor equations of motion is as follows:

$$\begin{cases} F_x - f_x = m\ddot{x} \\ F_y - f_y = m\ddot{y} \\ T_e - T_L = J\dot{\omega}/P_M \end{cases} \tag{2}$$

where m is the mass of the rotor, g the gravity constant, J the rotational inertia, ω the rotor angular velocity, and T_L the load.

2.3. Analysis of the Generalized Inverse

In order to realize the decoupling control among speed and radial displacements of the ORC-BPMSM, this paper uses the Interactor algorithm to construct the inverse system. Speed ω and radial displacement x and y are used as the output variables of the inverse system, as $\mathbf{Y} = [y_1, y_2, y_3]^T = [x, y, \omega]^T$, meanwhile $\mathbf{X} = [x_1, x_2, x_3, x_4, x_5]^T = [x, y, \dot{x}, \dot{y}, \omega]^T, \mathbf{U} = [u_1, u_2, u_3, u_4]^T = [i_{Md}, i_{Mq}, i_{Bd}, i_{Bq}]$ as status and input variables, respectively.

Firstly, each component of the output variable Y is derived until the input variable U is explicit in the derived expression, as seen in Equation (3). The Jacobi matrix is obtained by Equation (3). As can be seen in Equation (4), the rank is 3, and the relative order is $\alpha = (\alpha_1, \alpha_2, \alpha_3) = (2, 2, 1)$, satisfying the condition $\alpha_1 + \alpha_2 + \alpha_3 \leq 5$ (5 is the number of state variables). It can be seen that the inverse system of the original system exists, and the inverse system function expressions are shown in Equation (5).

$$\begin{cases} \dot{y}_1 = \dot{x}_1 = x_3 \\ \ddot{y}_1 = \ddot{x}_1 = \dot{x}_3 = K(L_{Md}u_1u_3 + \psi_f u_3 + L_{Mq}u_2u_4)/m + Cx_1/m \\ \dot{y}_2 = \dot{x}_2 = x_4 \\ \ddot{y}_2 = \ddot{x}_2 = x_4 = K(L_{Md}u_1u_4 + \psi_f u_4 - L_{Mq}u_2u_3)/m + Cx_2/m - g \\ \dot{y}_3 = \dot{x}_5 = \dfrac{3}{2J}P_M^2\psi_f u_2 - \dfrac{P_M}{J}T_L \end{cases} \tag{3}$$

$$\mathbf{A}(x) = \left[\frac{\partial(\ddot{y}_1, \ddot{y}_2, \dot{y}_3)}{\partial U}\right] = \frac{K}{m} \cdot \begin{bmatrix} L_{Md}u_3 & L_{Mq}u_4 & L_{Md}u_1 + \psi_f & L_{Mq}u_2 \\ L_{Md}u_4 & -L_{Mq}u_3 & -L_{Mq}u_2 & L_{Md}u_1 + \psi_f \\ 0 & \dfrac{3}{2JK}P_M^2\psi_f & 0 & 0 \end{bmatrix} \tag{4}$$

$$\mathbf{U} = [u_1, u_2, u_3, u_4]^T = \xi\left(X, \ddot{y}_1, \ddot{y}_2, \dot{y}_3\right) \tag{5}$$

Further, assume that the V shown in Equation (6):

$$V = [y_1, \dot{y}_1, y_2, \dot{y}_2, y_3] \tag{6}$$

Then the derivative Jacobi matrix of $\mathbf{V}$ with respect to $\mathbf{X}^T$ can be expressed as shown in Equation (7):

$$\det\left(\frac{\partial \mathbf{V}}{\partial \mathbf{X}^T}\right) = \begin{bmatrix} 1 & 0 & 0 & 0 & 0 \\ 0 & 0 & 1 & 0 & 0 \\ 0 & 1 & 0 & 0 & 0 \\ 0 & 0 & 0 & 1 & 0 \\ 0 & 0 & 0 & 0 & 1 \end{bmatrix} = -1 \tag{7}$$

According to the theory of uniqueness of implicit function, $\mathbf{X}$ can be uniquely represented by $\mathbf{V}$; therefore, the final expression of inverse system is shown in Equation (8).

$$\mathbf{U} = [u_1, u_2, u_3, u_4]^T = \bar{\xi}\left(y_1, \dot{y}_1, \ddot{y}_1, y_2, \dot{y}_2, \ddot{y}_2, y_3, \dot{y}_3\right) \tag{8}$$

In order to obtain an open-loop stable pseudo-linear system, a linear link is introduced in this paper, and the resulting generalized inverse expression is shown in Equations (9) and (10).

$$\begin{aligned} u &= \tilde{\varphi}\left(\left\{y_1, y_1', y_2, y_2', y_3\right\}, \hat{v}\right) \\ \hat{v} &= (v_1, v_2, v_3)^T \end{aligned} \tag{9}$$

$$\begin{cases} v_1 = a_{10}y_1 + a_{11}\dot{y}_1 + a_{12}\ddot{y}_1 \\ v_2 = a_{20}y_2 + a_{21}\dot{y}_2 + a_{22}\ddot{y}_2 \\ v_3 = a_{30}y_3 + a_{31}\dot{y}_3 \end{cases} \tag{10}$$

In order to decouple the system into a pseudo-linear system consisting of two second-order radial displacement subsystems and one first-order rotational speed subsystem, taking $\alpha_{10} = 1$, $\alpha_{11} = 1.414$, $\alpha_{12} = 1$, $\alpha_{20} = 1$, $\alpha_{21} = 1.414$, $\alpha_{22} = 1$, $\alpha_{30} = 1$, $\alpha_{31} = 1$, the expected transfer function of the obtained pseudo-linear subsystems is

$$\begin{cases} G_1 = \dfrac{1}{s^2 + 1.414s + 1} \\ G_2 = \dfrac{1}{s^2 + 1.414s + 1} \\ G_3 = \dfrac{1}{s + 1} \end{cases} \tag{11}$$

The generalized inverse system is connected in series before the ORC-BPMSM system to form a specific generalized inverse pseudo-linear composite system.

3. DECOUPLING CONTROL BASED ON LS-SVM GENERALIZED INVERSE

3.1. LS-SVM

In LS-SVM, for a given set of training samples, given a samples, $D = \{(x_i, y_i), i = 1, 2, \ldots, n, x_i \in \mathbf{R}^m, y_i \in \mathbf{R}\}, x_i$ and y_i are input and output matrices, respectively. The nonlinear mapping $\varphi(x)$ maps the samples from the original space to high-dimensional feature space.

$$\mathbf{y} = \boldsymbol{\omega}^T \boldsymbol{\phi}\left(\mathbf{x}\right) + \mathbf{b} \tag{12}$$

where ω is the weight matrix, and $\mathbf{b}$ is the offset value.

According to the principle of structural risk minimization, the optimization problem is defined as:

$$\min \mathbf{J}\left(\boldsymbol{\omega}, \mathbf{e}\right) = \frac{1}{2}\left\|\boldsymbol{\omega}\right\|^2 + \frac{1}{2}\gamma \sum_{i=1}^{n} \mathbf{e}_i^2 \tag{13}$$

$$y_i = \boldsymbol{\omega}^T \boldsymbol{\phi}\left(x_i\right) + b + e_i, i = 1, 2, \cdots, n \tag{14}$$

where $\mathbf{J}$ is the penalty function, γ the regularization parameter, and $\mathbf{e}_k$ the fitting error of the loss function.

The solution of the optimization problem with Lagrange function is as follows:

$$\mathbf{L}(\mathbf{w}, \mathbf{b}, \mathbf{e}, \boldsymbol{\alpha}) = \mathbf{J}(\mathbf{w}, \mathbf{e}) - \sum_{i=1}^{n} \alpha_i \left[\mathbf{w}^T \boldsymbol{\phi}(\mathbf{x}_i) + \mathbf{b} + \mathbf{e}_i - \mathbf{y}_i\right] \tag{15}$$

where α_i isthe Lagrangian multiplier, $i = 1, 2, \ldots, n$, $\mathbf{a} = [a_1, a_2, \ldots, a_n]^T$, $\mathbf{e} = [e_1, e_2, \ldots, e_n]^T$.

According to the KTT (Karush-Kuhn-Tucker) condition, the partial derivative of (15) is obtained and equal to zero,

$$\begin{cases} \dfrac{\partial L}{\partial \mathbf{w}} = 0 \rightarrow \mathbf{w} = \displaystyle\sum_{i=1}^{n} \boldsymbol{\alpha}_i \boldsymbol{\phi}(\mathbf{x}_i) \\ \dfrac{\partial L}{\partial \mathbf{b}} = 0 \rightarrow \displaystyle\sum_{i=1}^{n} \boldsymbol{\alpha}_i = 0 \\ \dfrac{\partial L}{\partial e_i} = 0 \rightarrow \boldsymbol{\alpha}_i = \gamma \mathbf{e}_i \\ \dfrac{\partial L}{\partial \boldsymbol{\alpha}_i} = 0 \rightarrow \mathbf{w}^T \boldsymbol{\phi}(\mathbf{x}_i) + \mathbf{b} + \mathbf{e}_i - \mathbf{y}_i = 0 \end{cases} \tag{16}$$

The analytical solution can be obtained according to formula (16):

$$\begin{bmatrix} \mathbf{b} \\ \mathbf{a} \end{bmatrix} = \begin{bmatrix} 0 & \mathbf{I}_n^{\mathbf{T}} \\ \mathbf{I}_n & \boldsymbol{\Omega} + \lambda^{-1}\mathbf{I} \end{bmatrix}^{-1} \begin{bmatrix} 0 \\ \mathbf{y} \end{bmatrix} \tag{17}$$

where $\mathbf{y} = [y_1, y_2, \ldots, y_n]^T$, $\mathbf{I}_n = [1, 1, \ldots, 1]^T$, $\boldsymbol{\Omega}$ is a square matrix and $\boldsymbol{\Omega} = \{\Omega_{ij}\}_{n\times n} = K(\mathbf{x}_i, \mathbf{x}_j) = \boldsymbol{\phi}(\mathbf{x}_i)^T \cdot \boldsymbol{\phi}(\mathbf{x}_j)$, $K(\mathbf{x}_i,\ \mathbf{x}_j)$ is the kernel function which satisfies Mercer theorem. In this paper, the radialbasis kernel function $K(\mathbf{x}_i, \mathbf{x}) = \exp\left(-\|\mathbf{x} - \mathbf{x}_i\| / 2\sigma^2\right)$ is used for kernel function.

Ultimately, the final regression function of the inverse model is:

$$\mathbf{y}(\mathbf{x}) = \sum_{i=1}^{n} \boldsymbol{\alpha}_i K(\mathbf{x}_i, \mathbf{x}) + \mathbf{b} \tag{18}$$

From formula (18), the LS-SVM function fitting structure is shown in the Figure 2.

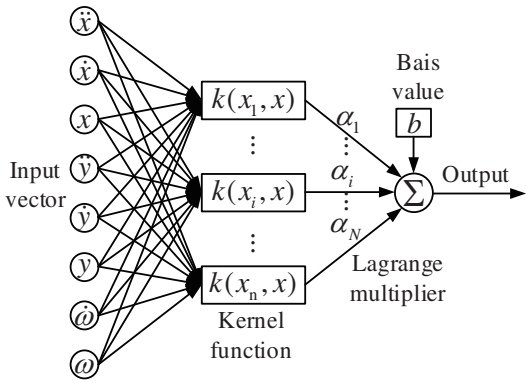

Figure 2. Structure of the LS-SVM function fitting.

3.2. Inverse Model Identification of LS-SVM

When building a generalized inverse model with LS-SVM, the selection of parameter σ^2 and regularization parameter γ of kernel function determines the performance of the generalized inverse

model. Therefore, in order to improve the accuracy of the inverse model, the network search method is used to optimize the parameters γ and σ^2 of LS-SVM.

For the ORC-BPMSM, the specific steps of building its generalized inverse model by using LS-SVM are as follows:

(i) The control system of ORC-BPMSM is constructed by using the Rotor Field Oriented Control method. Through inputting the random excitation signal, obtaining the operation data of corresponding radial displacement of x-, y-directions and rotational speed ω and obtaining the excitation signal $\{i_{Md}, i_{Mq}, i_{Bd}, i_{Bq}\}$. Sampling time is set to 0.1 ms, and running time is 100 ms. After multiple running and sampling, 1000 sets of data are obtained, of which 600 sets are used as training samples, and the remaining 400 sets are used as test samples. According to the generalized inverse system theory, it is necessary to calculate the generalized derivative of the radial displacement of x-, y-directions and rotational speed ω, from which the obtained data sets x, $(1+s)x$, $(1+1.414s+s^2)x$, y, $(1+s)y$, $(1+1.414s+s^2)y$, ω, $(1+s)\omega$ are normalized form the training sample of LS-SVM together with the excitation signal $\{i_{Md}, i_{Mq}, i_{Bd}, i_{Bq}\}$. To reduce the training error and increase the training speed, the obtained data is normalized into -1 to 1.

(ii) The initial population of parameters (γ, σ^2) is selected firstly using the grid search method, and the LS-SVM generalized inverse model is trained separately using this initial population, then using this model to test the test samples. The unsuitable parameters will be eliminated according to the overall test error, generating the next generation of parameter populations. Repeat the above steps until the test error meets the training accuracy. The parameters of LS-SVM are $\gamma = 3000$, $\sigma = 12$. Training three LS-SVMs can gain the corresponding α_i and b, then according to the input formula (18) can identify the output of the generalized inverse model.

(iii) The LS-SVM generalized inverse system fitting output characteristics are tested with the rotor radial displacement, shown in Figure 3, where the solid line is the actual output radial displacement of the system model simulation, and the dotted line is the LS-SVM generalized inverse system tracking output of the motor. As can be seen from Figure 3, the LS-SVM generalized inverse system can achieve the displacement fitting output of the system very well, which indicates that the inverse system obtained from the training is accurate and reliable.

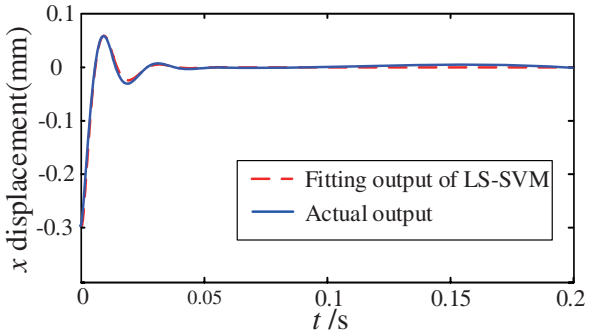

Figure 3. LS-SVM sample data fitting.

(iv) After obtaining the generalized inverse system identified by LS-SVM, it is connected in series with the original system to form a generalized inverse pseudo-linear composite system of ORC-BPMSM, and the system is coupled into three relatively independent pseudo linear subsystems, as shown in Figure 4.

(v) Design linear closed-loop controllers for each pseudo linear subsystem. The position subsystems are two second-order linear systems; the position regulators in the x- and y-directions use a PID controller; the speed subsystem is a first-order system; and the speed controller uses a PI regulator. The control structure of the ORC-BPMSM is shown in Figure 5.

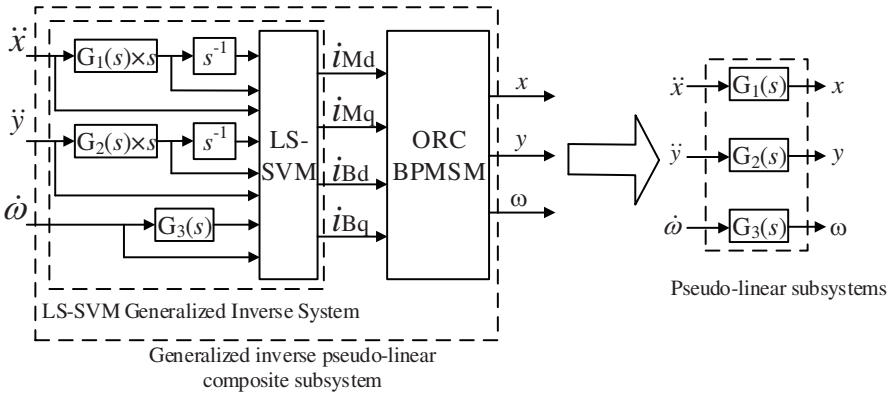

Figure 4. Pseudo-linear system structure.

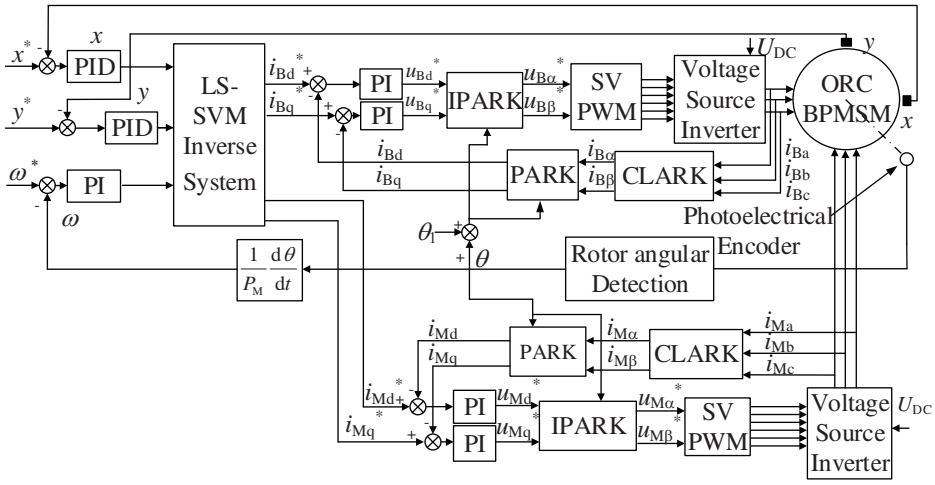

Figure 5. The control structure of the ORC-BPMSM.

4. SIMULATION TEST

To verify the effectiveness of the proposed control method, take ORC-BPMSM as the research object. The proposed method is compared with the inverse system control method in the Matlab/Simulink environment. In simulation, the flux of the permanent magnet is 0.125 Wb; torque windings pole-pair is 3; the resistance value is 2.326 Ω; the suspension windings pole-pair is 2; the resistance value is 1.65 Ω; the initial position of the motor rotor is $x = -0.3$ mm, $y = -0.2$ mm.

4.1. Decoupling Control Performance among Speed and Radial Displacements

Figure 6 shows the speed change curve and radial displacement curves in the x- and y-directions when the motor speed is suddenly accelerated from 2000 r/min to 3000 r/min, respectively. It can be seen from Figure 6 that the proposed method reaches the target speed 3000 r/min at 30 ms, that both x and y radial displacements are not affected by the sudden change during the speed change, and that the rotor is still in central stable suspension. The inverse system method (IS-based method) reaches the target speed 3000 r/min at 35 ms; speed response produces an overshoot of 25 r/min; and during the sudden change of speed, the peak-to-peak values of the rotor fluctuation in the x- and y-directions are 19 μm and 21 μm, respectively. The comparison of the simulation results shows that the proposed method has faster and more accurate speed regulation performance, and the change of torque has very little effect on the suspension force. The decoupling among torque and suspension forces is realized.

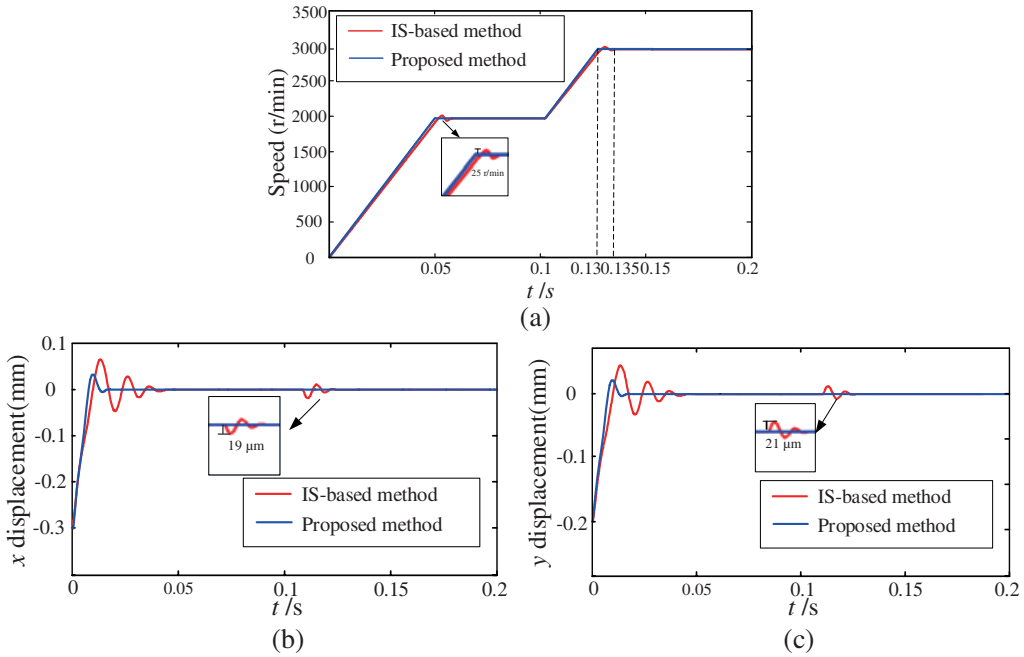

Figure 6. Speed and displacement curves of the decoupling control performance among the suspension forces and the electromagnetic torque in the comparative simulation. (a) Speed. (b) Displacement in the x direction. (c) Displacement in the y direction.

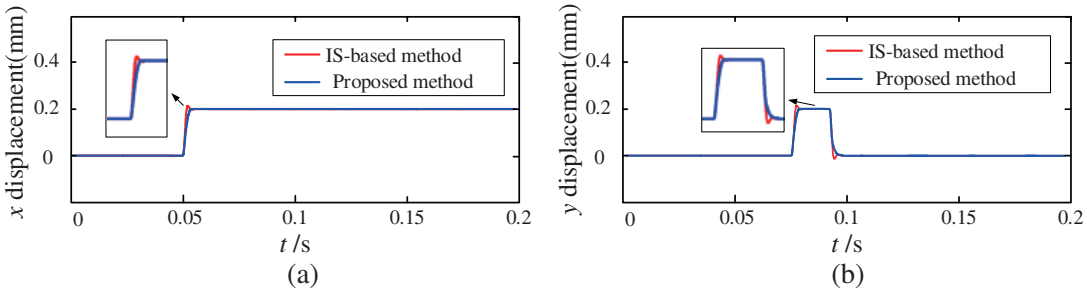

Figure 7. Displacement curves of the decoupling control performance between radial displacements. (a) Displacement in the x direction. (b) Displacement in the y direction.

4.2. Decoupling Control Performance between Displacements in the x- and y-direction

Figure 7 shows the curves of comparative decoupling performance between radial displacements. After the rotor is running in stable stage at the equilibrium position, a 0.2 mm step signal lasting 150 ms is applied in the x direction of the rotor, at $t = 0.05$ s, and the 0.2 mm step signal which lasts 20 ms is applied in the y direction of the rotor at $t = 0.075$ s. It can be seen from Figure 7 that when one variable changes it does not cause the other variable to change, which indicates that both control methods can achieve dynamic decoupling between the radial displacements, but the proposed method has smaller overshoot and better tracking performance than the IS-based control method.

4.3. Anti-Interference Performance Comparison

Figure 8 shows anti-interference performance comparison simulation curves with given speed of 3000 r/min, 30 N interference force applied in the x direction at 0.1 s, and 30 N interference force applied in the y direction at 0.16 s. As can be seen in Figure 8, the peak-to-peak values of the curves which

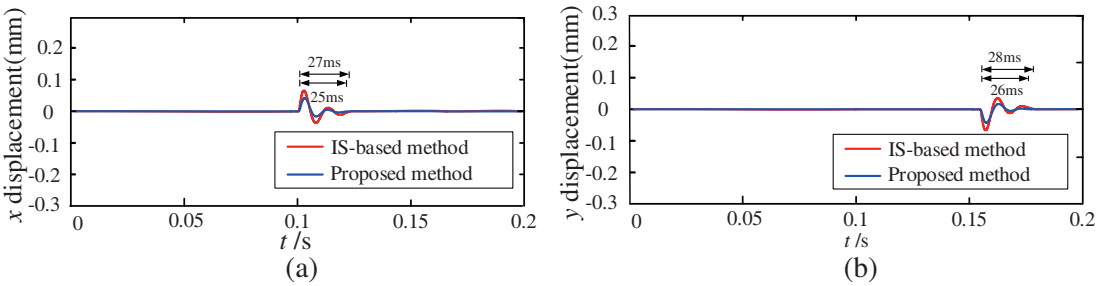

Figure 8. Displacement curves of the anti-interference performance. (a) Displacement in the x direction. (b) Displacement in the y direction.

adopts IS-based method in the x- and y-direction are 65 µm and 44 µm, respectively. The peak-to-peak values of the curves which adopts the proposed method in the x- and y-directions decrease to 41 µm and 28 µm, and the regulation time of the rotor recovering suspending stably is less than that of the IS-based method. Comparing the simulation results, the system has better interference resistance and robustness under the proposed method than the control method of IS-based method.

5. EXPERIMENTAL RESEARCH

To verify the feasibility of the proposed method, an ORC-BPMSM phototype is used to conduct a comparative experimental study. The DSPTMS320F28335 is used as the core digital controller for the experiments, and the experimental platform includes ORC-BPMSM phototype, power drive circuit board, DSP system, eddy current sensors, interface circuits, etc. The experimental platform is shown in Figure 9.

The TMS320F28335 is used to generate PWM signals, which drive two power boards to achieve the control of the ORC-BPMSM torque windings and suspension windings currents. Eddy current sensors are used to detect the displacement signals which are input to DSP after being processed by the interface circuit, then the closed-loop control of displacement is achieved. The photoelectric encoder is used to gain the rotational speed signals.

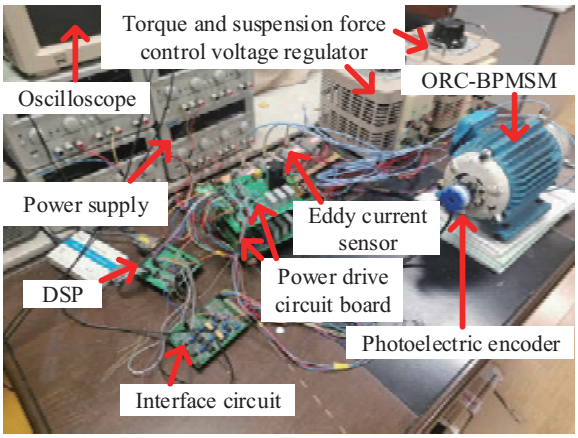

Figure 9. Experimental platform of the ORC-BPMSM.

5.1. Variable Speed Experiment

Figure 10 shows the comparative experimental waveforms using the two kind of control methods when the rotational speed is changed. As seen in Figure 10(a), when the IS-based method is used, the speed

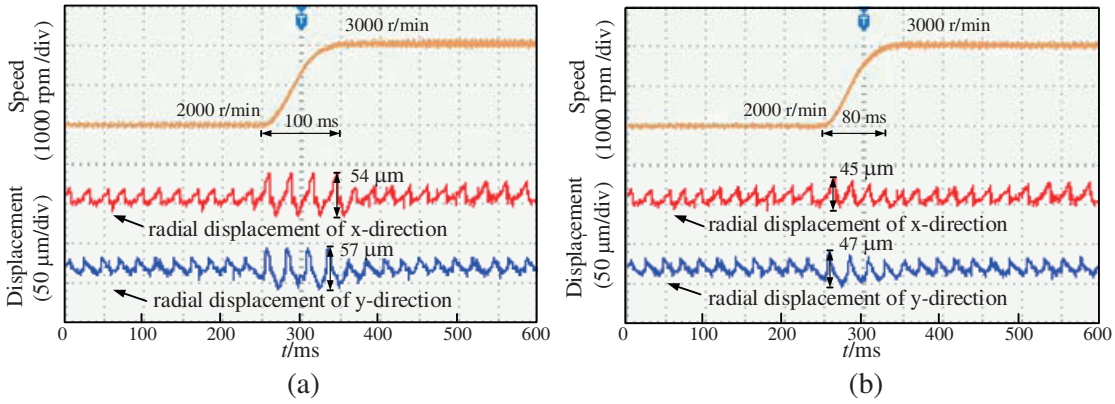

Figure 10. Speed response curve and corresponding radial displacement waveforms. (a) IS-based method, (b) proposed method.

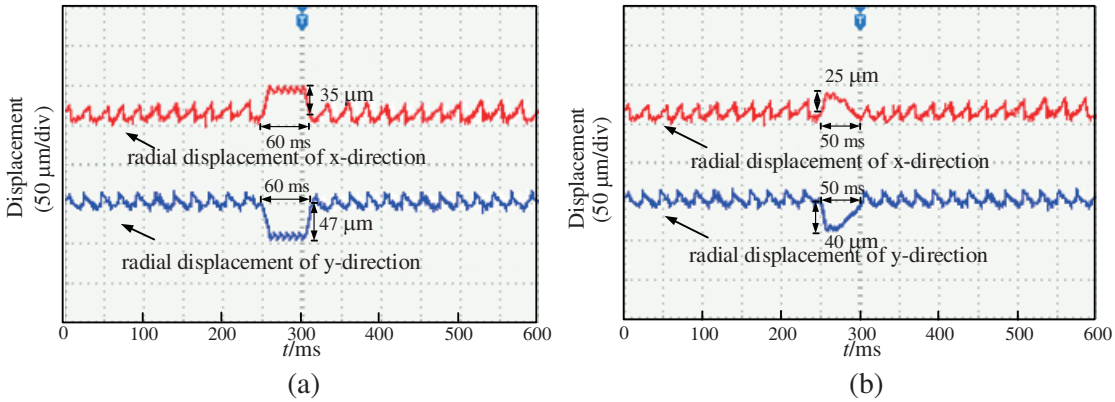

Figure 11. Radial displacement waveforms under disturbing force. (a) IS-based method, (b) proposed method.

rises from 2000 r/min to 3000 r/min; the response time is 100 ms; the radial displacements of the rotor in the x- and y-direction are 54 μm and 57 μm, respectively. As seen in Figure 10(b), the proposed method is used; the response time for adjusting the speed is 80 ms; and the radial displacements of the rotor in the x- and y-directions are 45 μm and 47 μm, respectively; during the speed changing process, the radial displacements in the x- and y-directions are continuously decreasing, and finally stabilize at the equilibrium position. Comparing the experimental results, the proposed control method has better speed regulation performance and better decoupling control among speed and radial displacements than the control method of IS-based method.

5.2. Decoupling Control Performance between Displacements in the x- and y-direction

Figure 11 shows the comparative experimental waveforms using the two control methods when the disturbance force 10N is applied in the y direction. As seen in Figure 11(a), because of the couple between x- and y-directions, the maximum displacement deviation in the x direction is about 35 μm, and the stable operation of the rotor is restored after 60 ms. As seen in Figure 11(b), the maximum displacement deviation in the x direction is about 25 mm, and the stable operation of the rotor is restored after the adjustment time of 50 ms. Comparing the experimental results, the proposed control method can make the system have stronger decoupling performance than the control method of IS-based method.

6. CONCLUSIONS

In this paper, an decoupling method based on LS-SVM generalized inverse is proposed to realize decoupling control of the ORC-BPMSM among speed and displacements. The ORC-BPMSM system is proved reversible by establishing mathematical models and reversibility analysis. The generalized inverse system of the original system is identified by LS-SVM, then the pseudo-linear system is formed by connecting the original system with the inverse system. Moreover, closed-loop controllers are designed to improve the stability and robustness of the whole motor drive system. Finally, simulation results show that the proposed control method has better decoupling performance and anti-interference performance than the inverse system, and experiment results show that the proposed control method has good and dynamic decoupling performance.

ACKNOWLEDGMENT

This work was supported by National Natural Science Foundation of China (61973144).

REFERENCES

1. Sun, X.-D., L. Chen, and Z.-B. Yang, "Overview of bearingless permanent-magnet synchronous motors," *IEEE Trans. Ind. Electron.*, Vol. 60, No. 12, 55285538, 2013.
2. Zhu, H.-Q. and Y. Xu, "Permanent magnet parameter design and performance analysis of bearingless flux switching permanent magnet motor," *IEEE Trans. Ind. Electron.*, Vol. 68, No. 5, 4153–4163, 2020.
3. Ooshima, M., S. Kobayashi, and H. Tanaka, "Magnetic suspension performance of a bearingless motor/generator for flywheel energy storage systems," *IEEE Pes. General Meeting*, Vol. 29, No. 18, 100–105, 2010.
4. Ooshima, M., S. Kitazawa, and A. Chiba, "Design and analyses of a coreless-stator type bearingless motor/generator for clean energy," *IEEE INTERMAG 2006*, Vol. 34, No. 9, 1360–1367, 2014.
5. Zhi, L., Y.-L. Xu, and X.-F. Yang, "Generalized inverse multiplicative structure for differential-equation-based hysteresis models," *IEEE Trans. Ind. Electron.*, Vol. 68, No. 5, 4182–4189, 2021.
6. Huang, H.-B., J.-H. Wu, X.-R. Huang, M.-L. Yang, and W.-P. Ding, "A generalized inverse cascade method to identify and optimize vehicle interior noise sources," *Journal of Sound and Vibration*, Vol. 467, 115062, 2020.
7. Sun, X.-D., L. Chen, and H. Jiang, "High-performance control for a bearingless permanent-magnet synchronous motor using neural network inverse scheme plus internal model controllers," *IEEE Trans. Ind. Electron.*, Vol.63, No. 6, 1–1, 2016.
8. Zhu, H.-Q. and W. Du, "Decoupling control of bearingless permanent magnet synchronous motor based on inverse system using the adaptive neural-fuzzy inference system," *Proceedings of the CSEE*, Vol. 39, No. 4, 1190–1197, 2019.
9. Zhu, H.-Q. and Z.-W. Gu, "Active disturbance rejection control of 5-degree-of-freedom bearingless permanent magnet synchronous motor based on fuzzy neural network inverse system," *ISA Trans.*, Vol. 101, 2020.
10. Liu, G.-H. and R.-J. Chen, "Model-free adaptive robust control for two motor drive system based on neural network inversion," *Proceedings of the CSEE*, Vol. 39, No. 3, 868–874, 2019.
11. Cao, F., T. Yang, Y. Li, and S. Tong, "Adaptive neural inverse optimal control for a class of strict feedback stochastic nonlinear systems," *2019 IEEE 8th Data Driven Control and Learning Systems Conference (DDCLS)*, 432–436, doi: 10.1109/DDCLS.2019.8908901, 2019.
12. Shi, Q. and H. Zhang, "Fault diagnosis of an autonomous vehicle with an improved SVM algorithm subject to unbalanced datasets," *IEEE Trans. Ind. Electron.*, Vol. 68, No. 7, 6248–6256, 2020.
13. Zhao, W.-X., X.-Q. Qiu, and G.-H. Liu, "Internal model control of linear permanent-magnet vernier motor based on support vector machines generalized inverse," *Control and Decision*, Vol. 31, No. 8, 1419–1423, 2016.

14. Wang, Z.-Q. and X.-L. Huang, "Nonllinear decoupling control for bearingless induction motor based on support vector machines inversion," *Transactions of China Electrotechnical Society*, Vol. 30, No. 10, 164–170, 2015.
15. Toledo-Pérez, D. C., J. Rodríguez-Reséndiz, R. A. Gómez-Loenzo, and J. C. Jauregui-Correa, "Support vector machine-based EMG signal classification techniques: A review," *Appl. Sci.*, Vol. 9, 4402, 2019.
16. Vapnik, V., *The Nature of Statistical Learning Theory*, Springer, New York, NY, 1995.
17. Suykens, J.-A.-K. and J. Vandewalle, "Recurrent least squares support vector machines," *IEEE Trans. Circuits Syst. I: Fundamental Theory and Appl.*, Vol. 47, No. 7, 1109–1114, 2000.